

# *Correlated Bayesian Additive Regression Trees with Gaussian Process for Regression Analysis of Dependent Data*

Xuetao Lu <sup>a\*</sup> and Robert E. McCulloch <sup>b</sup>

<sup>a</sup> Department of Biostatistics, The University of Texas MD Anderson Cancer Center

<sup>b</sup> School of Mathematical and Statistical Sciences, Arizona State University

\* Author for correspondence: robert.mcculloch@asu.edu

## Abstract

Bayesian Additive Regression Trees (BART) has gained widespread popularity, prompting the development of various extensions for different applications. However, limited attention has been given to analyzing dependent data. Based on a general correlated error assumption and an innovative dummy representation, we introduce a novel extension of BART, called Correlated BART (CBART), designed to handle correlated errors. By integrating CBART with a Gaussian process (GP), we propose the CBART-GP model, in which the CBART and GP components are loosely coupled, allowing them to be estimated and applied independently. CBART captures the covariate mean function  $E[y|\mathbf{x}] = f(\mathbf{x})$ , while the Gaussian process models the dependency structure in the response  $y$ . We also developed a computationally efficient approach, named two-stage analysis of variance with weighted residuals, for the estimation of CBART-GP. Simulation studies demonstrate the superiority of CBART-GP over other models, and a real-world application illustrates its practical applicability.

*Keywords:* non-linearity, non-parametric model, BART, MCMC, spatial regression.

## 1 Introduction

Bayesian Additive Regression Trees (BART) ([Chipman et al., 2010](#)) is effective to explore nonlinear relationships, showing comparable performance to other widely used machine learning algorithms ([Chipman et al., 2006](#)). In BART, the regression of a response variable on a vector of covariates is modeled as a sum-of-trees function plus an error term. A key assumption is the errors following an independent and identically distributed (i.i.d.) zero mean normal distribution. Studies on extensions to accommodate more general error distributions have been conducted. [Pratola et al. \(2020\)](#) employ a second ensemble of trees to model heteroskedastic errors, while [George et al. \(2019\)](#) use Dirichlet process mixtures for nonparametric error modeling. For comprehensive reviews of BART and its extensions,

see [Piegorisch et al. \(2022\)](#) and [Hill et al. \(2020\)](#). However, above BART extensions still rely on the independent assumption, limiting the applicability of BART in dependent data analysis. In this paper, we consider the dependent errors, following a multivariate zero-mean normal distribution with a general covariance matrix  $\Sigma$ . Under this framework, BART and its aforementioned extensions can be seen as special cases where  $\Sigma$  are diagonal matrices. We introduce an innovative dummy representation that converts a regression tree to a linear regression model to work with the general form of  $\Sigma$ . This results in matrix operations dominating the MCMC computations, necessitating an efficient algorithm, which is another contribution of this paper. We refer to this new BART model as "Correlated BART" and denote it as CBART for brevity. Simulation studies demonstrate that CBART can effectively estimate the underlying true (nonlinear) regression function  $E[y|\mathbf{x}] = f(\mathbf{x})$ , i.e., the relationship between covariates  $\mathbf{x}$  and response  $y$ , when provided with the true  $\Sigma$ .

One typical class of covariance matrix  $\Sigma$  can be defined by a kernel function  $\Sigma_{i,j} = K(s_i, s_j|\theta)$ , where  $\theta$  denotes the set of parameters,  $s_i$  and  $s_j$  are labels (e.g., time or spatial points) of random samples  $Y(s_i)$  and  $Y(s_j)$ . The random samples,  $Y(s_1), \dots, Y(s_n)$ , together is called a Gaussian process (GP) ([Rasmussen and Williams, 2005](#)) which is widely applied in the fields of time series ([Roberts et al., 2012](#); [Brahim-Belhouari and Bermak, 2004](#)) and spatial statistics ([Kriging, 1951](#); [Cressie, 1993](#)). [Gramacy and Lee \(2008\)](#) introduced treed Gaussian processes (tGP) that combine stationary GPs with a single tree to model nonstationary dependence through treed partitioning. [Starling et al. \(2020\)](#) proposed tsBART, which integrates BART with GPs to enhance smoothness over target covariates. [Maia et al. \(2024\)](#) developed GP-BART, where BART and GPs collaborate to model spatial dependence. In these methods, a Gaussian Process (GP) is applied in each tree leaf instead of a simple mean function. GPs serve as fundamental building blocks in model estimation, which are tightly coupled with the tree and BART. Both tGP and GP-BART, similar to machine learning models such as random forest, may overfit the dependent structure in the data, which can compromise their ability to accurately estimate the true function  $E[y|\mathbf{x}] = f(\mathbf{x})$ . In many circumstances, the estimation of  $E[y|\mathbf{x}] = f(\mathbf{x})$  that facilitates the interpretation of how covariates affect the response is more important than merely fitting the data well. Regression kriging models ([Stein and Corsten, 1991](#)) are designed for this purpose.

Combining CBART with a Gaussian process, we introduce CBART-GP, a novel regression model designed for analyzing dependent data. CBART-GP utilizes CBART to model the function  $E[y|\mathbf{x}] = f(\mathbf{x})$  and a GP to capture the dependency structure in the response. This model stands out from tGP, tsBART, and GP-BART by integrating CBART with a single GP in a loosely coupled way, enabling independent estimation of CBART and GP. This brings CBART-GP two advantages. First and most important, by separately modeling the data dependency in GP, CBART ensures accurate estimation of the true function  $E[y|\mathbf{x}] = f(\mathbf{x})$ . Meanwhile, it also achieves precise predictions by combining CBART and GP together. In contrast, methods like BART, tGP, GP-BART, and traditional machine learning models typically excel only in one of the two aspects. Additionally, unlike regression kriging which assumes  $f(\mathbf{x})$  is in the form of linear regression, CBART can adapt well to nonlinear scenarios of  $f(\mathbf{x})$ . Secondly, CBART-GP does not impose restrictions on the parameterization of GP, unlike GP-BART which uses a fixed exponentiated-quadratic kernel. This flexibility allows the adaptation of different parameterizations for various data types such as time series and spatial data. To keep the loose coupling between CBART and GP, we developed a method of two-stage analysis of variance with weighted residuals for estimating the CBART-GP model. Simulation studies demonstrate the effectiveness of this method.

In Section 2, we introduce the CBART model, including dummy representation, MCMC updating, efficient matrix computations, and an example illustrating the similarity and difference between BART and CBART. Section 3 details the CBART-GP model, describing its components and introducing a two-stage analysis of variance with weighted residuals method for model estimation. Section 4 presents simulation studies to demonstrate the effectiveness of CBART-GP. In Section 5, we apply CBART-GP to a real-world spatial dataset. A short discussion is made in section 6. We have implemented the proposed model and algorithm in an R package, "CbartGP", which is available at <https://github.com/lxtpvt/CbartGP>.

## 2 Correlated BART

Consider  $\{Y, X\} = \{y_i, X_i = (x_{1i}, \dots, x_{pi})\}_{i=1}^n$  are observations of a univariate response and a  $p$ -dimensional vector of predictors, the BART model posits as follows:

$$y_i = \sum_{j=1}^m g(X_i; T_j, M_j) + \epsilon_i, \quad \epsilon_i \stackrel{\text{i.i.d.}}{\sim} N(0, \sigma^2), \quad (1)$$

where  $g(X_i; T_j, M_j)$  is a step function,  $T_j$  denotes a binary tree consisting of a set of decision rules and a set of terminal nodes,  $M_j = \{\mu_{j1}, \dots, \mu_{jb_j}\}$  represents a set of mean values associated with the terminal nodes of  $T_j$ .

From (1), we know that BART is defined as a sum of binary regression trees. Figure 1 shows an example of the tree,  $Y = g(X; T, M)$ , in which we have  $Y = \{y_1, \dots, y_5\}$ ,  $X = \{X_1, \dots, X_5\}$  and  $X_i = (x_{1i}, x_{2i})$ .  $T$  including the rules at interior nodes and  $M = \{\mu_1, \mu_2, \mu_3\}$  comprising the means of terminal nodes are shown in panel (a). The step function  $g(X; T, M)$  is depicted in panel (b).

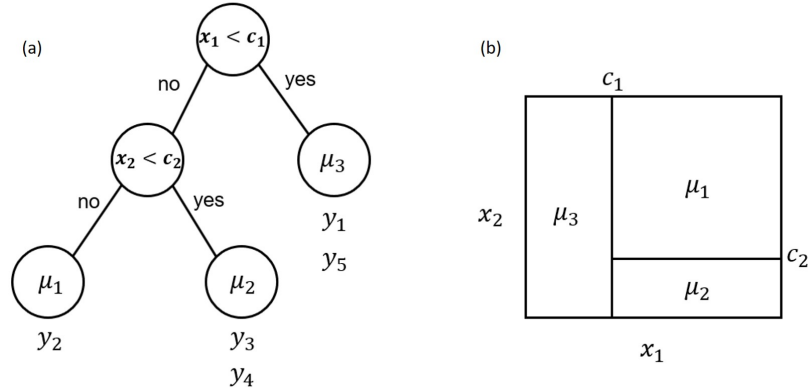


Figure 1: An example of binary regression tree model. (a) Tree structure includes the set of interior nodes with decision rules ( $T$ ) and the set of parameter values associated with terminal nodes. (b) The step function  $g(X, T, M)$  is depicted by the corresponding partition of the sample space.

In BART model (1), the errors are assumed  $\epsilon_i \stackrel{\text{i.i.d.}}{\sim} N(0, \sigma^2)$ . This assumption may not hold in general, for example, in modeling time series or spatial data. Therefore, we extend this assumption by allowing the errors could correlate with each other. Let  $\Sigma$  denote a

general covariance matrix, the correlated BART (CBART) can be defined as follows:

$$Y = \sum_{j=1}^m g(X; T_j, M_j) + \epsilon, \quad \epsilon \sim N(0, \Sigma), \quad (2)$$

where  $Y = \{y_1, \dots, y_n\}$ ,  $X = \{X_1, \dots, X_n\}$ ,  $g(X; T_j, M_j) = \{g(X_1; T_j, M_j), \dots, g(X_n; T_j, M_j)\}$ , and  $\epsilon = \{\epsilon_1, \dots, \epsilon_n\}$ .

## 2.1 Dummy Representation

Similar to BART, the building block of CBART is the binary regression tree. In order to handle the covariance matrix, we propose the concept of dummy representation as follows:

*Definition 2.1* (Dummy representation).

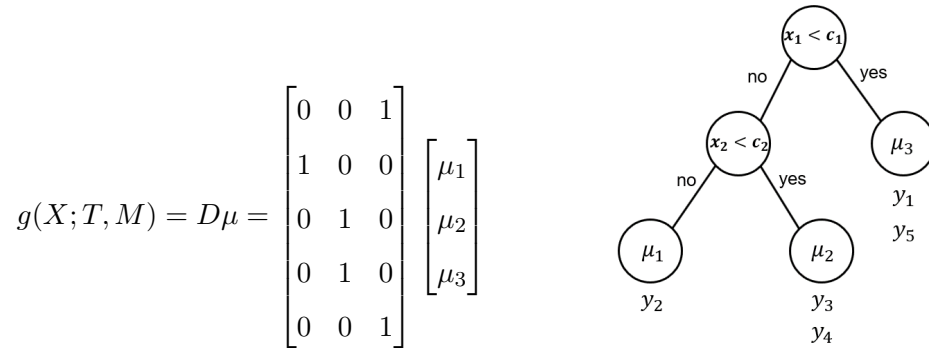
$$g(X; T, M) = D\mu \quad (3)$$

where

$$D = \begin{bmatrix} d_{11} & d_{12} & \dots & d_{1b} \\ d_{21} & d_{22} & \dots & d_{2b} \\ \vdots & \vdots & \ddots & \vdots \\ d_{n1} & d_{n2} & \dots & d_{nb} \end{bmatrix}, \quad \mu = [\mu_1, \mu_2, \dots, \mu_b]^T.$$

In the matrix  $D$ , each row contains zeros in all entries except for the one linked to the bottom node to which the observation is mapped. For example, the  $i^{th}$  row in  $D$ ,  $[d_{i1}, \dots, d_{i,j-1}, d_{i,j}, d_{i,j+1}, \dots, d_{in}] = [0, \dots, 0, 1, 0, \dots, 0]$ , demonstrates that the  $i^{th}$  observation was mapped to the  $j^{th}$  bottom node.

As an example, the dummy representation of binary regression tree in Figure 1 is shown as follows. The matrix multiplication serves to map  $\{y_2\}$  to  $\mu_1$ ,  $\{y_3, y_4\}$  to  $\mu_2$ , and  $\{y_1, y_5\}$  to  $\mu_3$ .



Based on dummy representation, a binary regression tree can be denoted as the following matrix form.

$$Y = g(X; T, M) + \epsilon = D\mu + \epsilon, \quad \epsilon \sim N(0, \Sigma). \quad (4)$$

## 2.2 Bayesian Backfitting and Markov Chain Monte Carlo

To fit the BART model in (1), Chipman et al. (2006, 2010) proposed a Bayesian backfitting (Hastie and Tibshirani, 2000) approach, using MCMC to update the pair  $(T_j, M_j)$  conditioned on  $\sigma^2$  and the remaining trees. For CBART, we need to deal with  $\Sigma$  instead of  $\sigma^2$ , such that the backfitting reparameterization can be presented as follows:

$$R_j = Y - \sum_{k \neq j} g(X; T_k, M_k) = g(X; T_j, M_j) + \epsilon, \quad \epsilon \sim N(0, \Sigma). \quad (5)$$

It is easy to check that (5) denotes an individual binary regression tree. As the subscript  $j$  can take any value in  $\{1, \dots, m\}$ , without loss of generality, we simplify the notation (5) by omitting the subscript hereafter.

$$R = g(X; T, M) + \epsilon, \quad \epsilon \sim N(0, \Sigma). \quad (6)$$

The key step in BART's MCMC is to update  $(T, M)$  given  $(R, \Sigma)$ . Since we know  $p(T, M|R, \Sigma) = p(M|T, R, \Sigma)p(T|R, \Sigma)$ , the problem can be converted to the following steps:

$$T|R, \Sigma \quad (7)$$

$$M|T, R, \Sigma \quad (8)$$

### (1) Updating $T$ through Metropolis-Hastings algorithm

Chipman et al. (1998) introduced Metropolis-Hastings algorithm for updating  $T$  in (7). A Markov chain updates the states of the tree in a sequence as follows :

$$T^0, T^1, T^2, \dots$$

Starting from an initial state  $T^0$ , the state transition from  $T^i$  to  $T^{i+1}$ ,  $i = 0, 1, 2, \dots$ , follows two steps:

- Given the current state  $T^i$ , generate a candidate state  $T^*$  according to the transition kernel  $q(T^i, T^*)$ .

- Set  $T^{i+1} = T^*$  with the probability,

$$\alpha(T^{i+1} = T^*) = \min\left\{\frac{q(T^*, T^i)}{q(T^i, T^*)} \frac{p(R|X, T^*)p(T^*)}{p(R|X, T^i)p(T^i)}, 1\right\}. \quad (9)$$

Otherwise, set  $T^{i+1} = T^i$ .

The terms  $q(T^*, T^i), q(T^i, T^*), p(T^*), p(T^i)$  in (9) are chosen in the same way as for BART. The part that is different between BART and CBART is the marginal likelihood ratio:

$$\frac{p(R|X, T^*)}{p(R|X, T^i)} = \frac{p(R|X, T^{i+1})}{p(R|X, T^i)}. \quad (10)$$

Given  $\Sigma$ , based on the dummy representation of (4), we have that

$$p(R|X, T) = p(R|D) = \int p(R|D, \mu)\pi(\mu) d\mu, \quad (11)$$

where

$$p(R|D, \mu) \sim N(D\mu, \Sigma), \quad \pi(\mu) \sim N(\bar{\mu}, Q^{-1}), \quad (12)$$

mean  $\bar{\mu}$  and precision matrix  $Q$  are pre-specified hyperparameters.

**Theorem 2.2** (Marginal distribution of  $p(R|D)$ ). *Given (11) and (12), the marginal distribution  $p(R|D)$  can be expressed as follows:*

$$p(R|D) = \frac{(2\pi)^{-\frac{n}{2}} |\Sigma|^{-\frac{1}{2}} |Q|^{\frac{1}{2}}}{|Q + D^T \Sigma^{-1} D|^{\frac{1}{2}}} \exp\left\{-\frac{1}{2}(-v^T(Q + D^T \Sigma^{-1} D)v + \bar{\mu}^T Q \bar{\mu} + R^T \Sigma^{-1} R)\right\} \quad (13)$$

where,  $v = (Q + D^T \Sigma^{-1} D)^{-1}(Q\bar{\mu} + D^T \Sigma^{-1} R)$ .

Similar to BART, (13) can be simplified by setting  $\bar{\mu} = 0$  as follows:

$$p(R|D) = \frac{(2\pi)^{-\frac{n}{2}} |\Sigma|^{-\frac{1}{2}} |Q|^{\frac{1}{2}}}{|Q + D^T \Sigma^{-1} D|^{\frac{1}{2}}} \exp\left\{\frac{1}{2}[R^T \Sigma^{-1} D(Q + D^T \Sigma^{-1} D)^{-1} D^T \Sigma^{-1} R - R^T \Sigma^{-1} R]\right\} \quad (14)$$

See proof in Appendix A.

Based on Theorem 2.2, the marginal likelihood ratio (10) is denoted as follows:

$$\begin{aligned} \frac{p(R|X, T^{i+1})}{p(R|X, T^i)} &= \frac{p(R|D^{i+1})}{p(R|D^i)} = \frac{|Q^{i+1}|^{\frac{1}{2}}}{|Q^i|^{\frac{1}{2}}} \frac{|Q^i + (D^i)^T \Sigma^{-1} D^i|^{\frac{1}{2}}}{|Q^{i+1} + (D^{i+1})^T \Sigma^{-1} D^{i+1}|^{\frac{1}{2}}} \\ &\exp\left\{\frac{1}{2}R^T \Sigma^{-1} [D^{i+1}(Q^{i+1} + (D^{i+1})^T \Sigma^{-1} D^{i+1})^{-1} (D^{i+1})^T - \right. \\ &\quad \left. D^i(Q^i + (D^i)^T \Sigma^{-1} D^i)^{-1} (D^i)^T] \Sigma^{-1} R\right\} \end{aligned} \quad (15)$$

where the superscript  $i$  and  $i + 1$  corresponds to state  $i$  and state  $i + 1$ , respectively.

## (2) Updating $M$ through the posterior of $\mu$

Based on the following Theorem 2.3, we can update  $M$  in (8) by drawing  $\mu$  from its posterior distribution.

**Theorem 2.3** (Posterior distribution of  $\mu$ ).

$$p(\mu|R) \sim N((Q + D^T \Sigma^{-1} D)^{-1}(Q\bar{\mu} + D^T \Sigma^{-1} R), (Q + D^T \Sigma^{-1} D)^{-1}) \quad (16)$$

Let  $\bar{\mu} = 0$ , it can be simplified to

$$p(\mu|R) \sim N((Q + D^T \Sigma^{-1} D)^{-1} D^T \Sigma^{-1} R, (Q + D^T \Sigma^{-1} D)^{-1}). \quad (17)$$

See proof in Appendix A.

## 2.3 Efficient Matrix Computations

In the MCMC of BART, computations in (15) and (17) are efficient because of the assumption of i.i.d. errors, i.e.,  $\Sigma = \sigma^2 I$ . However, due to the general form of  $\Sigma$ , in CBART these computations become intensive as the number of observations  $n$  increases.

For a deeper understanding of the computation complexity, let's set

$$A = Q + D^T \Sigma^{-1} D, \quad (18)$$

which is a  $b \times b$  symmetric matrix and  $b$  is the number of bottom nodes. Given matrix  $A$ , the computation of  $|A|$  and  $A^{-1}$  in (15) and (17) require  $O(b^3)$  operations. As CBART (same to BART) prefers small trees, where the number of bottom nodes,  $b$ , is typically less than 20, the complexity of  $O(b^3)$  is manageable when  $A$  is known. However, challenges arise in the calculation of  $A$ , where  $\Sigma^{-1}$  needs  $O(n^3)$  operations. For a large number of observations, e.g.,  $n > 10^5$ , this computation becomes infeasible for most computers. Fortunately, in some applications such as time series and spatial data analysis,  $\Sigma$  exhibits sparsity, i.e., most of its entries are zeros. In such cases, the computation complexity can be reduced through some well designed algorithms/methods which have been extensively studied in both applied mathematics (Hackbusch, 2015; Lin et al., 2011) and statistics (Datta et al., 2016; Finley et al., 2019; Litvinenko et al., 2019). The most favorable outcome is reducing the complexity from  $O(n^3)$  to  $O(n)$ .



The special structure of the matrix  $D$  in dummy representation offers an opportunity to improve the computation efficiency of marginal likelihood ratio (15). The idea is to reorder  $D$  into a block matrix and apply block computation techniques to enhance efficiency. The definition of reordering is as follows:

*Definition 2.4* (Reordering). The matrix  $D$  in dummy representation (3) can be reordered to a block matrix  $D_P$  using a permutation matrix  $P$ ,

$$D = PD_P, \quad P^T D = D_P, \quad (19)$$

where

$$D_P = \begin{bmatrix} d'_{11} & d'_{12} & \dots & d'_{1b} \\ d'_{21} & d'_{22} & \dots & d'_{2b} \\ \vdots & \vdots & \ddots & \vdots \\ d'_{n1} & d'_{n2} & \dots & d'_{nb} \end{bmatrix}, \quad d'_{ij} = \begin{cases} 0, & i \notin \Omega_j, \\ 1, & i \in \Omega_j. \end{cases} \quad i = 1, \dots, n; \quad j = 1, \dots, b,$$

$\Omega_j$  is the index set of observations that be mapped to  $j^{th}$  bottom node.

Recalling the example shown in Figure 1, reordering can be demonstrated as follows:

$$D = \begin{bmatrix} 0 & 0 & 1 \\ 1 & 0 & 0 \\ 0 & 1 & 0 \\ 0 & 1 & 0 \\ 0 & 0 & 1 \end{bmatrix} = PD_P = \begin{bmatrix} 0 & 0 & 0 & 0 & 1 \\ 1 & 0 & 0 & 0 & 0 \\ 0 & 1 & 0 & 0 & 0 \\ 0 & 0 & 1 & 0 & 0 \\ 0 & 0 & 0 & 1 & 0 \end{bmatrix} \begin{bmatrix} 1 & 0 & 0 \\ 0 & 1 & 0 \\ 0 & 1 & 0 \\ 0 & 0 & 1 \\ 0 & 0 & 1 \end{bmatrix}.$$

For consistency, it is imperative to simultaneously reorder  $\{D, R, \Sigma\}$  to  $\{D_P, R_P, \Sigma_P\}$  using the same permutation matrix  $P$ , as follows:

$$D = PD_P, \quad R = PR_P, \quad \Sigma = P\Sigma_P P^T. \quad (20)$$

Then, we can prove that the marginal likelihood ratio (15) is invariant under reordering by the following Theorem.

**Theorem 2.5** (Reordering invariance). *Reordering does not change the value of the marginal*

likelihood ratio in (15).

$$\begin{aligned} \frac{p(R|D^{i+1})}{p(R|D^i)} &= \frac{|Q^{i+1}|^{1/2}}{|Q^i|^{1/2}} \frac{|Q^i + (D_P^i)^T \Sigma_P^{-1} D_P^i|^{1/2}}{|Q^{i+1} + (D_P^{i+1})^T \Sigma_P^{-1} D_P^{i+1}|^{1/2}}. \\ &\exp\left\{\frac{1}{2} R_P^T \Sigma_P^{-1} [D_P^{i+1} (Q^{i+1} + (D_P^{i+1})^T \Sigma_P^{-1} D_P^{i+1})^{-1} (D_P^{i+1})^T \right. \\ &\quad \left. - D_P^i (Q^i + (D_P^i)^T \Sigma_P^{-1} D_P^i)^{-1} (D_P^i)^T] \Sigma_P^{-1} R_P\right\} \end{aligned} \quad (21)$$

See proof in Appendix A.

The steps of calculating marginal likelihood ratio (21) can be found in B. Given  $\Sigma^{-1}$ , by leveraging the block matrix computation technique, the complexity of computing (21) can be reduced from  $O(n^2)$  to  $\max\{O(n), O(b^2)\}$ .

## 2.4 Example: comparison of BART and CBART

The data for this example is generated from the following model:

$$y_i = f(x_i) + \eta_i, \quad i \in \{1, \dots, n\}, \quad (22)$$

where  $n = 200$ ,  $f(x_i) = x_i^3$  and  $x_i$  is sampled from a uniform distribution in  $(-1, 1)$ . Let  $\boldsymbol{\eta} = \{\eta_1, \dots, \eta_n\}$  and assume  $\boldsymbol{\eta} \sim N(0, \Sigma)$ .  $\eta_i$  is generated as follows:

$$\eta_1 = \epsilon_1, \quad \eta_i = \rho * \eta_{i-1} + \epsilon_i, \quad 0 \leq \rho < 1, \quad i = 2, \dots, n.$$

where  $\epsilon_i \stackrel{\text{i.i.d.}}{\sim} N(0, \sigma^2)$ ,  $i = 1, \dots, n$ . We have the matrix form  $A\boldsymbol{\eta} = \boldsymbol{\epsilon}$ , where

$$A = \begin{bmatrix} 1 & \dots & \dots & 0 & 0 \\ -\rho & 1 & \dots & 0 & 0 \\ \vdots & \ddots & \ddots & \vdots & \vdots \\ 0 & \dots & \ddots & 1 & 0 \\ 0 & \dots & \dots & -\rho & 1 \end{bmatrix}_{n \times n}, \quad \boldsymbol{\eta} = \begin{bmatrix} \eta_1 \\ \vdots \\ \eta_n \end{bmatrix}, \quad \boldsymbol{\epsilon} = \begin{bmatrix} \epsilon_1 \\ \vdots \\ \epsilon_n \end{bmatrix}. \quad (23)$$

Thus, by  $\boldsymbol{\eta} = A^{-1}\boldsymbol{\epsilon}$ , we can obtain that

$$\Sigma = \text{var}(\boldsymbol{\eta}) = A^{-1} \text{var}(\boldsymbol{\epsilon}) [A^{-1}]^T = \sigma^2 A^{-1} [A^{-1}]^T, \quad \Sigma^{-1} = \sigma^{-2} A^T A.$$

BART was estimated directly from the data using the usual MCMC and default prior. The posterior mean of the error standard deviation was 0.1. For both BART and CBART,  $f(x)$  is estimated with the posterior mean of the MCMC draws of  $f$  evaluated at  $x$ . Both

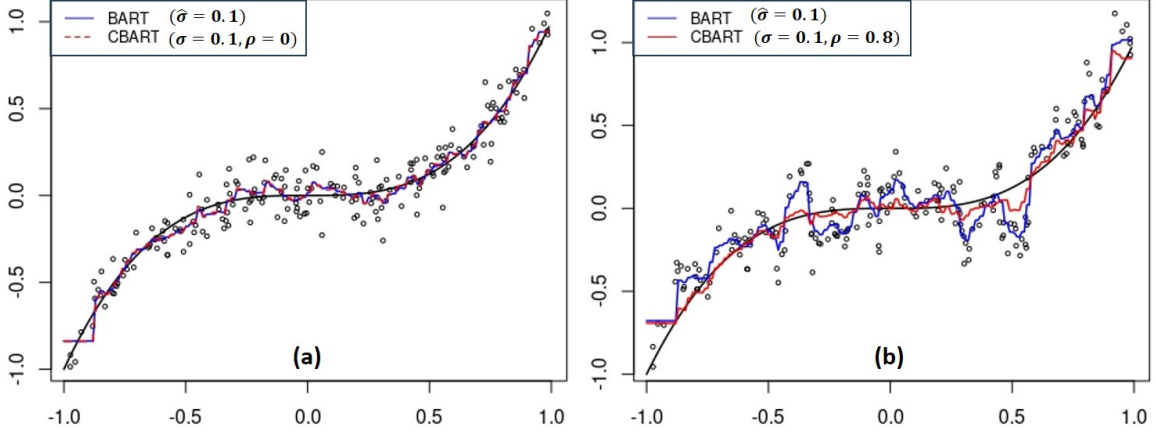


Figure 2: Panel (a) illustrates the the posterior means of  $E[y|x] = f(x)$  estimated from CBART and BART by MCMC when the errors are i.i.d. Panel (b) highlights the distinction between CBART and BART and shows the ability of CBART in estimating the true  $f(\mathbf{x})$  when the errors are correlated.

BART and CBART use the same priors on the trees but CBART uses  $\Sigma$  with  $\sigma = 0.1$  and  $\rho = 0$  or  $0.8$ .

In panel (a) with  $\rho = 0$ , CBART and BART are the same except that BART estimates the error variance. We see that the estimates of  $f(x)$  are virtually identical. However, in the scenario where the errors are correlated, as illustrated in panel (b), BART tends to overfit the errors, resulting in poor performance in capturing  $f(x)$ . Conversely, with the true parameters  $\sigma = 0.1$  and  $\rho = 0.8$ , CBART effectively reduces overfitting and provides an accurate estimation of the  $f(x)$ . In practice, the true parameters  $(\sigma, \rho)$  are unknown. We will introduce a method to estimate them in Section 3.2.

### 3 CBART-GP: CBART with Gaussian Process

Motivated by regression Kriging in spatial statistics, we employ a Gaussian process to capture dependencies in the residuals of the response. Integrating CBART with GP, we propose the model CBART-GP. Unlike regression Kriging, CBART-GP can manage non-linear regression functions, thus broadening its applicability in practice.

### 3.1 Model Specification

CBART-GP and its components are outlined as follows:

$$y(s_i) = f_{CBART}(\mathbf{x}(s_i)) + \eta(s_i|\theta), \quad i = 1, 2, \dots, n. \quad (24)$$

- $s_i$ : the label of observations, e.g., time or location for time series or spatial data;
- $y(s_i)$ : the observed response at  $s_i$ ;
- $\mathbf{x}(s_i)$ : the observed covariates at  $s_i$ ;
- $\eta(s_i|\theta)$ : a Gaussian process with parameters  $\theta$ .

The Gaussian process  $\eta(s_i|\theta)$  can be tailored to different applications by choosing an appropriate parametrization. For example, for time series, it can be parameterized to an AR(p) model:

$$\eta(s_i) = a_1\eta(s_{i-1}) + \dots + a_p\eta(s_{i-p}) + \epsilon_i, \quad \epsilon_i \sim N(0, \tau^2). \quad (25)$$

In this case,  $\theta = \{a_1, \dots, a_p, \tau^2\}$ . We have discussed an example of the AR(1) model in Section 2.4.

For spatial data,  $\eta(s_i|\theta)$  can be parameterized as follows:

$$\eta(s_i) = z(s_i) + \epsilon_i, \quad \epsilon_i \sim N(0, \tau^2), \quad (26)$$

where  $z(s_i)$  is a zero mean stationary Gaussian process with Matérn covariance function,

$$Cov(z(s_i), z(s_j)) = \sigma^2 \frac{2^{1-\nu}}{\Gamma(\nu)} \left( \sqrt{2\nu} \frac{\|z(s_i) - z(s_j)\|^2}{\phi} \right)^\nu K_\nu \left( \sqrt{2\nu} \frac{\|z(s_i) - z(s_j)\|^2}{\phi} \right).$$

$\Gamma$  represents the gamma function,  $K_\nu$  denotes a modified Bessel function of the second kind.  $\nu$  is a predefined smoothness parameter, with popular choices being  $\nu \in \{1/2, 3/2, 5/2\}$ . In spatial statistics,  $\theta = \{\sigma^2, \phi, \tau^2\}$  are termed sill, range, and nugget, respectively.

### 3.2 Two-stage Analysis of Variance with Weighted Residuals

In tsBART and GP-BART, each tree leaf includes a GP functional, tightly coupling BART and GPs. In contrast, CBART-GP utilizes just one GP, which does not serve as a building block in the estimation of CBART. This setup is referred to as a loose coupling between

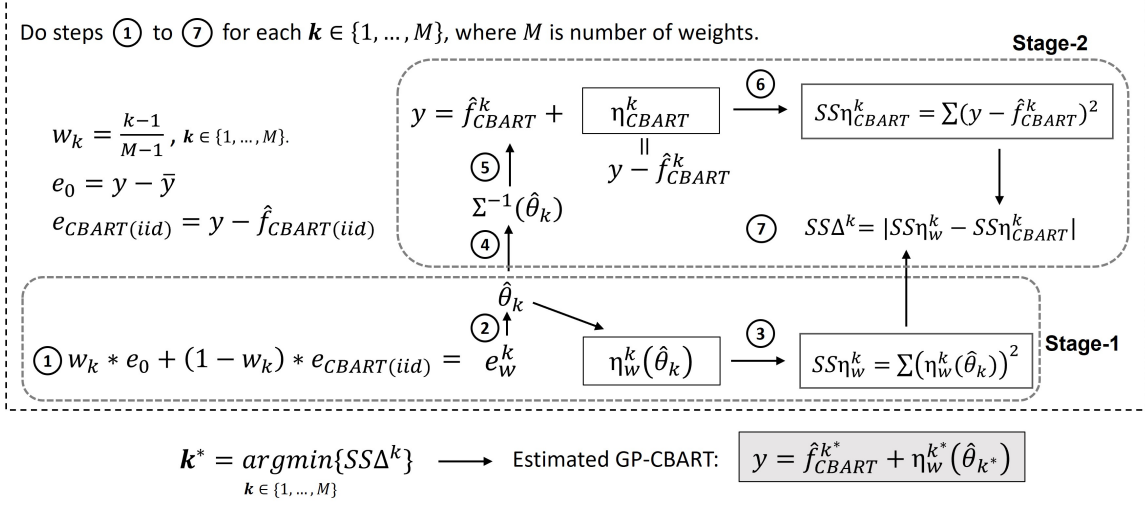


Figure 3: Steps and components of the two-stage analysis of variance with weighted residuals. The number of weights can be set as  $M = 6$ , which performed well in both simulations and real data applications in this paper.

CBART and GP. The loose coupling property offers two key advantages: (1) CBART retains its independence of estimating and using  $E[y|\mathbf{x}] = f(\mathbf{x})$ . (2) It provides greater flexibility in parameterizing  $\eta(\cdot|\theta)$ . Unlike GP-BART, which is limited to a quadratic covariance function, CBART-GP accommodates a range of parameterization strategies, as demonstrated in (25) and (26).

CBART is a nonparametric model capable of estimating arbitrary functions  $E[y|\mathbf{x}] = f(\mathbf{x})$ . Similarly, GP is also regarded as a nonparametric model that can capture the non-linear dependency structure of responses (without covariates  $\mathbf{x}$ ) across various spatial or temporal locations. Estimating these two models simultaneously presents a significant identification challenge. To overcome this challenge, we propose a method called two-stage analysis of variance with weighted residuals, which facilitates separate estimation of CBART and GP.

The steps and components of this approach are illustrated in Figure 3. The first stage is designed to estimate the GP,  $\eta(\cdot|\theta)$ , based on the idea that the dependent structure captured by the GP is contained in the residuals,  $e = y - \hat{f}(\mathbf{x})$ , where  $\hat{f}(\mathbf{x})$  is an estimation of  $f(\mathbf{x})$ . Two extreme examples are  $e_0 = y - \bar{y}$  and  $e_{CBART(iid)} = y - \hat{f}_{CBART(iid)}$ , where  $\hat{f}_{CBART(iid)}$  is the estimation from CBART assuming i.i.d. errors, which is equivalent to

BART. We regard  $e_0$  and  $e_{CBART(iid)}$  as representing the maximum and minimum of error dependency to be captured by the GP. Building on this, we introduce weighted residuals,  $e_w^k = w_k * e_0 + (1 - w_k) * e_{CBART(iid)}$ , to explore various degrees of dependency within the response. The steps ① to ③ in the first stage are outlined as follows:

Step ①: model the weighted residuals  $e_w^k = w_k * e_0 + (1 - w_k) * e_{CBART(iid)}$  with the parameterized GP model,  $e_w^k = \eta_w(\theta)$ .

Step ②: estimate the MLE  $\hat{\theta}_k$  (without  $\mathbf{x}$ ).

Step ③: calculate the variance in  $e_w^k$  explained by  $\eta_w^k(\hat{\theta}_k)$ , denoted as  $SS\eta_w^k$ .

The second stage focuses on estimating CBART and conducting the analysis of variance. Let  $\eta_{CBART}^k$  denote the GP model within CBART-GP and  $SS\eta_{CBART}^k$  represent the variance explained by  $\eta_{CBART}^k$ . The key idea is to align  $\eta_w^k(\hat{\theta}_k)$  as closely as possible with  $\eta_{CBART}^k$ . Their similarity is evaluated through the analysis of variance, aiming to minimize the difference,  $SS\Delta^k = |SS\eta_w^k - SS\eta_{CBART}^k|$ , where  $SS\eta_w^k = \sum(\eta_w^k(\hat{\theta}_k))^2$  and  $SS\eta_{CBART}^k = \sum(y - \hat{f}_{CBART}^k)^2$ . The steps from ④ to ⑦ in the second stage are detailed as follows:

Step ④: calculate the inverse covariance matrix  $\Sigma^{-1}(\hat{\theta}_k)$ .

Step ⑤: fit the CBART  $\hat{f}_{CBART}^k = \hat{f}(\mathbf{x}) = \hat{E}[y|\mathbf{x}]$  with  $\Sigma^{-1}(\hat{\theta}_k)$ .

Step ⑥: calculate  $SS\eta_{CBART}^k = \sum(y - \hat{f}_{CBART}^k)^2$  with fitted  $\hat{f}_{CBART}^k$ .

Step ⑦: calculate  $SS\Delta^k = |SS\eta_w^k - SS\eta_{CBART}^k|$ .

Finally, the optimal CBART-GP model is determined by identifying  $k^*$  that corresponds to the minimum  $SS\Delta^k$ .

To demonstrate the effectiveness of the two-stage analysis of variance with weighted residuals, let us revisit the example presented in Section 2.4. The weights for the residuals are given as  $\{w_1, w_2, w_3, w_4, w_5, w_6\} = \{0, 0.2, 0.4, 0.6, 0.8, 1\}$ , resulting in the following values for  $SS\Delta^k$ :  $\{1.733, 1.732, \mathbf{0.452}, 2.207, 6.221, 10.407\}$ . Among these, the minimum is  $SS\Delta^3 = 0.452$ . Thus, we can identify  $\hat{\theta}_3 = \{\hat{\rho}_3, \hat{\sigma}_3\} = \{0.810, 0.104\}$ , which are close approximations to the true values  $\theta = \{\rho, \sigma\} = \{0.800, 0.100\}$ . Correspondingly, as shown

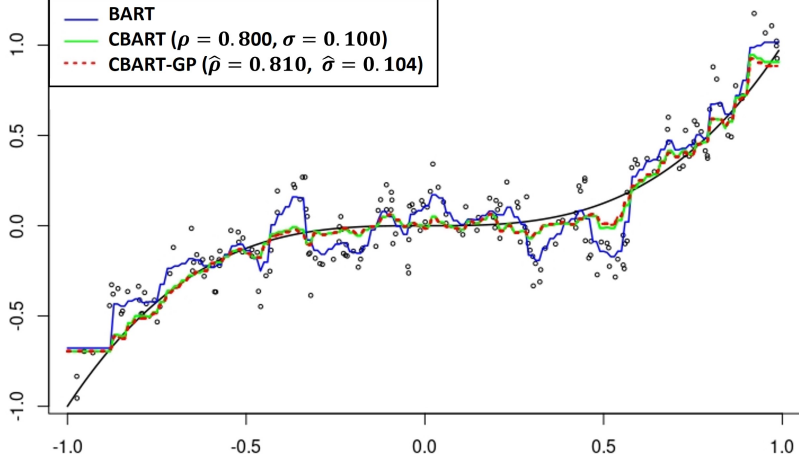


Figure 4: An example of parameter estimation using the two-stage analysis of variance with weighted residuals. We use the same example shown in Figure 2 panel (b).

in Figure 4, the CBART estimated using the two-stage method (the red dashed curve) demonstrates high consistency to the one (green solid curve) with true parameters.

The two-stage analysis of variance with weighted residuals is a hybrid approach, where the first stage employs maximum likelihood estimation for  $\eta_w(\hat{\theta}_k)$ , and the second stage utilizes Bayesian estimation (MCMC) for CBART. In contrast, we also considered a full Bayesian solution, which includes the following updates during each iteration of the MCMC.

$$\begin{aligned}
 (1) \quad & \sum_{j=1}^m \{T_j, M_j\} \mid \theta \Leftrightarrow \text{CBART} \mid \text{GP} \\
 (2) \quad & \theta \mid \sum_{j=1}^m \{T_j, M_j\} \Leftrightarrow \text{GP} \mid \text{CBART}
 \end{aligned} \tag{27}$$

where  $m$  is the number of trees. The full Bayesian solution presents three inherent limitations. First, since both CBART and GP are nonparametric and nonlinear, the full MCMC process becomes highly dependent in the updating of (27). Without strong prior information about the allocation of the fit between CBART and GP, it becomes challenging to identify both components simultaneously. Second,  $\eta(\theta)$  is integrated within the MCMC iterations, creating a tight coupling between the CBART and GP. Third, even though advanced techniques can reduce the computational complexity of calculating  $\Sigma^{-1}(\theta)$  from  $O(n^3)$  to  $O(n)$  in specific cases, the full Bayesian solution remains time-consuming due to the large number of iterations (e.g., 1000 iterations) typically required to maintain MCMC

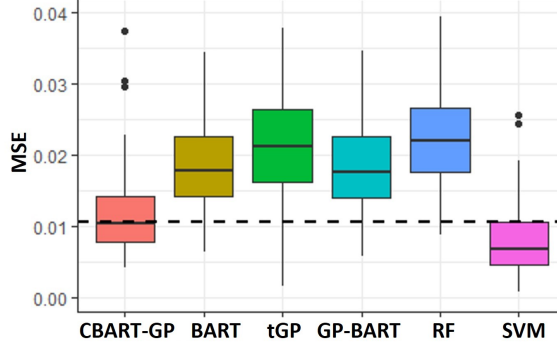


Figure 5: Model comparison in estimating the function  $E[y|x] = f(x)$ .

stationarity. In contrast, the two-stage method only necessitates a few calculations of  $\Sigma^{-1}(\theta)$  (specifically  $M = 6$  times), greatly decreasing the overall computational demand.

## 4 Simulation Studies

### 4.1 Estimation of $E[y|x] = f(x)$ with Dependent Errors

In Section 3.2, we provided an illustrative example to compare the performance of CBART-GP and BART in estimating the function  $f(x)$  under dependent errors by using the method of two-stage analysis of variance with weighted residuals. This section expands the comparison to include additional models: tGP, GP-BART, Random Forest (RF), and Support Vector Machine (SVM). We generated 100 different datasets using the same settings as those in Sections 2.4 and 3.2, each with a different seed. The results, displayed in Figure 5, show that the  $\hat{f}_{CBART}$  in CBART-GP outperforms all other models except for SVM. This underscores CBART-GP’s superiority in accurately revealing the underlying true function  $f(x)$  in the presence of correlated errors. Although SVM perform better than CBART-GP, it just simply ignores the dependent structure in the residuals. In contrast, CBART-GP handles this dependent structure via a GP, giving it an advantage over SVM, particularly in the prediction of spatial data discussed in the next section.

### 4.2 Spatial Data Analysis

Recall the parameterization for spatial data analysis in equation (26):

$$y(s_i) = f(x(s_i)) + \eta(s_i), \quad \eta(s_i) = z(s_i) + \epsilon_i,$$



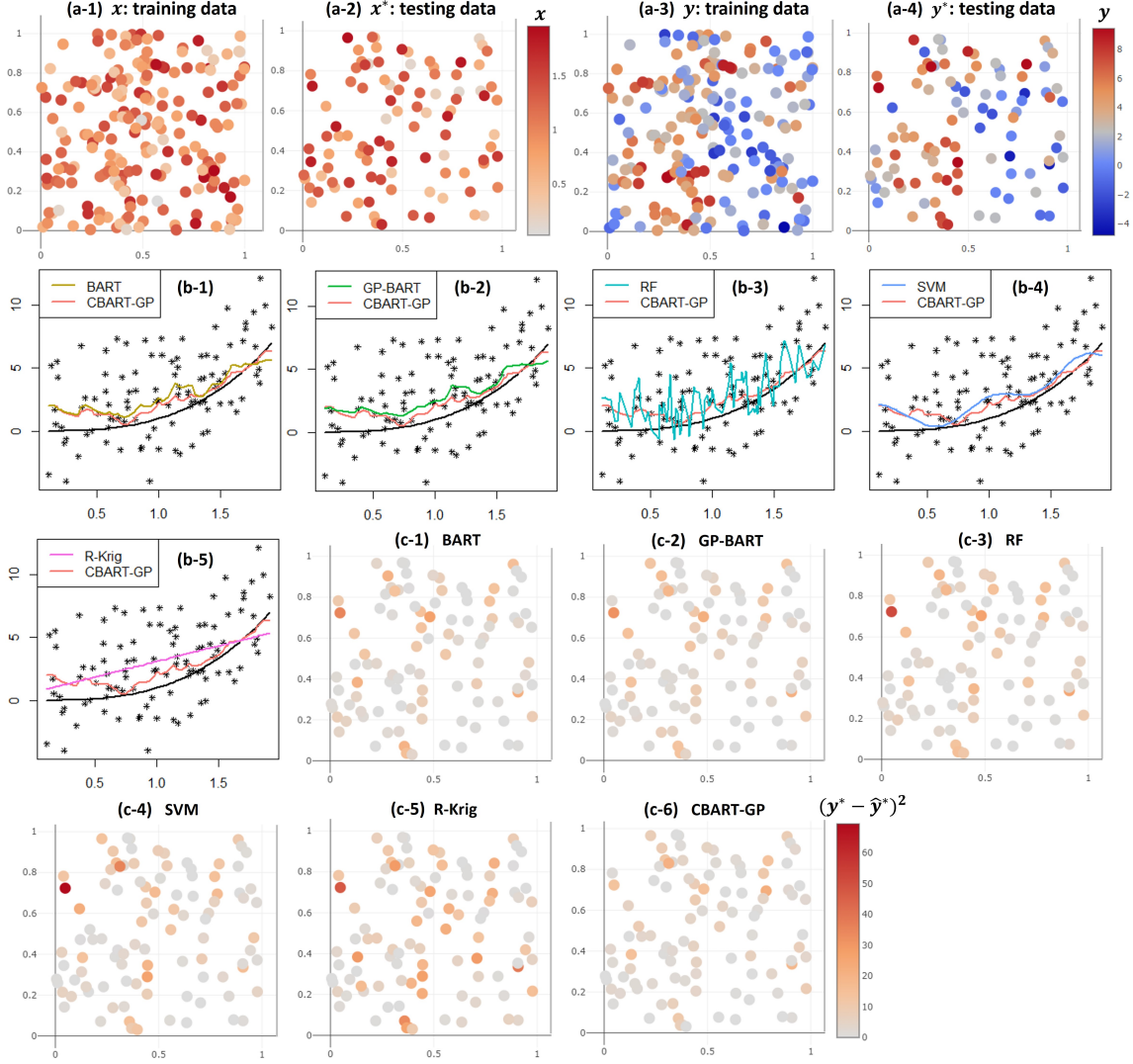


Figure 6: An example in the simulation of spatial data analysis. Panels (a-1) to (a-4): the training and testing datasets. Panels (b-1) to (b-5): comparison of estimating  $E[y|x] = f(x)$ . Panels (c-1) to (c-6): comparison of predicting new data  $y^*$ , which using the criterion of square of error,  $(y^* - \hat{y}^*)^2$ .

where  $s_i = (s_{i1}, s_{i2})$  represent a spatial point, and  $z(s_i)$  denote a Gaussian process  $GP(0, C(\cdot, \cdot | \theta))$  characterized by the covariance function  $C(\cdot, \cdot | \theta)$ . The independent and identically distributed (i.i.d.) errors  $\epsilon_i$  follow a normal distribution  $\epsilon_i \sim N(0, \tau^2)$ . Unlike the methods described in Section 4.1, spatial data analysis aims to achieve two primary goals: (1) estimating  $E[y|x] = f(x)$  to interpret the relationship between covariates and the response, and (2) predicting a new response  $y^*$  based on  $x^*$  and  $s^*$ . The CBART-GP

Table 1: The MSE reduction of CBART-GP comparing to other models in estimating  $E[y|x] = f(x)$  and predicting the new data  $y^*$ .

MSE reduction	BART	GP-BART	RF	SVM	R-Krig
$(\frac{MSE(\hat{f}) - MSE(\hat{f}_{CBART})}{MSE(\hat{f})} * 100)\%$	47.6%	50.0%	72.6%	24.7%	65.9%
$(\frac{MSE(\hat{y}^*) - MSE(\hat{y}_{CBART-GP}^*)}{MSE(\hat{y}^*)} * 100)\%$	21.6%	12.8%	28.8%	35.6%	52.6%

achieve these goals through: (1)  $E[y|x] = \hat{f}_{CBART}(x)$  for the goal of interpretation, and (2)  $\hat{y}^* = \hat{f}_{CBART}(x^*) + \hat{z}(s^*)$  for the goal of prediction. The performance of CBART-GP is compared with models: BART, GP-BART, RF, SVM, and Regression Kriging (R-Krig). For R-Krig, we have: (1)  $E[y|x] = \hat{\beta}x$  for interpretation, and (2)  $\hat{y}^* = \hat{\beta}x^* + \hat{z}(s^*)$  for prediction. For the remaining models, all represented as  $\hat{f}$ , we have: (1)  $E[y|x] = \hat{f}(x)$  for interpretation, and (2)  $\hat{y}^* = \hat{f}(x^*, s^*)$  for prediction. The tGP is excluded because it cannot handle cases where  $x^*$  and  $s^*$  are correlated, a scenario that may occur in practice. The settings for data generation are as follows:

- $s_i = (s_{i1}, s_{i2})$ , where  $s_{i1} \perp s_{i2}$  and be generated from the distribution  $unif(0, 1)$ .
- $z(s_i) \sim GP(0, C(\cdot, \cdot | \sigma, \phi))$ ,  $C(s_j, s_k | \sigma, \phi) = \sigma^2 \exp\{-\frac{d(s_j, s_k)}{\phi}\}$ , where  $d(s_j, s_k)$  is the Euclidean distance between the points  $s_j$  and  $s_k$ .
- $\epsilon_i \stackrel{\text{i.i.d}}{\sim} N(0, \tau^2)$ .
- The true parameters are  $\{\sigma^2, \phi, \tau^2\} = \{3, 6, 1\}$ .
- The true regression function is  $f(x(s_i)) = x(s_i)^3$ .
- $x(s_i)$  is generated to simulate three practical scenarios: (1)  $x(s_i)$  is entirely dependent on the spatial point  $s_i$ :  $x(s_i) = s_{i1} + s_{i2}$ . (2)  $x(s_i)$  is entirely independent of the spatial point  $s_i$ :  $x \sim 2 * unif(0, 1)$ . (3)  $x(s_i)$  exhibits a partial dependence and partial independence on the spatial point  $s_i$ :  $x(s_i) = 0.5 * (s_{i1} + s_{i2}) + unif(0, 1)$ .

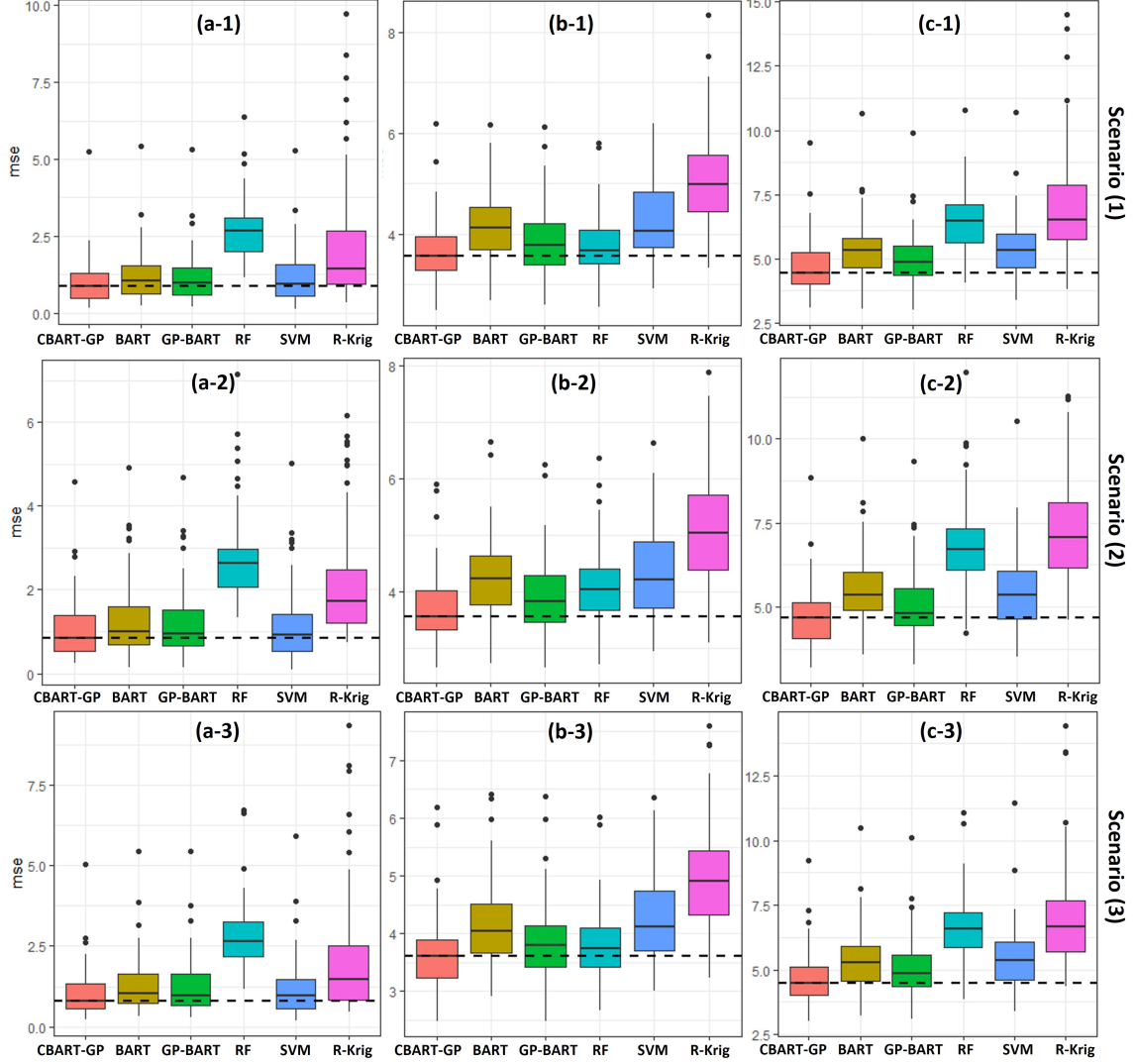


Figure 7: Simulation results of the spatial data analysis. Panels (a-1) to (a-3): The comparison in estimating  $E[y|x] = f(x)$ . Panels (b-2) to (b-3): The comparison in predicting new data  $y^*$ . Panels (c-1) to (c-3): The sum of first two columns, considering the two goals are equally important.

Similar to the one-dimensional simulation, we generate 100 different datasets (using different seeds) under each scenario of  $x(s_i)$ . Every dataset consists of 200 observations for training and 100 observations for testing. An example dataset of scenario (3) is depicted in panels (a-1) to (a-4) of Figure 6.

Using the example dataset, we can illustratively examine the models' performance in estimating  $E[y|x] = f(x)$  and predicting new data  $y^*$ . Panels (b-1) to (b-6) in Figure 6

exhibit the results of the former, where the comparisons with CBART-GP are also shown. CBART-GP performs better than other models. For predicting  $y^*$ , we can compare the models through the square of error,  $(y^* - \hat{y}^*)^2$ , as shown in panels (c-1) to (c-6). It is not difficult to find that CBART-GP outperforms other models as well. The quantitative measures of CBART-GP’s superiority can be found in Table 1.

The results of the spatial simulation are depicted in Figure 7. Interestingly, the outcomes across three scenarios are consistent, suggesting that spatial dependency of  $x$  does not significantly influence the models’ performance. Notably, CBART-GP demonstrates best performance in both estimating  $E[y|x] = f(x)$  and predicting new data  $y^*$ . While SVM performs comparably in the former task but poorly in the later.

## 5 Real Data Analysis

In this section, we apply CBART-GP to a real spatial dataset with 6213 observations, which came from the rapid carbon assessment project initiated by the Natural Resources Conservation Service’s Soil Science Division of the U.S. Department of Agriculture (Wijewardane et al., 2016). The response variable is the soil carbon stock, whose spatial distribution is illustrated in panel (a) of Figure 8. The dataset contains 31 environmental covariates. Among them, REDL14 (Landsat Band 3 (RED) 2014) and NDVI14 (Normalized Difference Vegetation Index 2014) exhibit nonlinear relationships with the response variable, as depicted in panels (b-1) and (b-2). Panels (c-1) and (c-2) present the observations in the three-dimensional space defined by the response variable and the two covariates. Our goal is to understand the effects of these two covariates on the response, i.e., estimate the true function  $E[y|\mathbf{x}] = f(x_{REDL14}, x_{NDVI14})$ . We compare the performance of CBART-GP with the models, BART, Random Forest, SVM, and Regression Kriging. tGP and GP-BART are excluded due to their intolerable computation time on this large dataset.

Panels (d-1,2) to (h-1,2) display the estimated functions  $E[y|\mathbf{x}] = \hat{f}(x_{REDL14}, x_{NDVI14})$  of different models from two angles. Considering the known nonlinear relationship between covariates and response, the regression Kriging estimation  $\hat{f}_{R-Krig}$  shown in panels (h-1,2) likely underestimates the true function. Conversely, the random forest estimation  $\hat{f}_{RF}$  in panels (f-1,2) appears to overestimate. The models BART and SVM yield similar estimations ( $\hat{f}_{BART}$  and  $\hat{f}_{SVM}$ ) in the areas indicated by the arrows

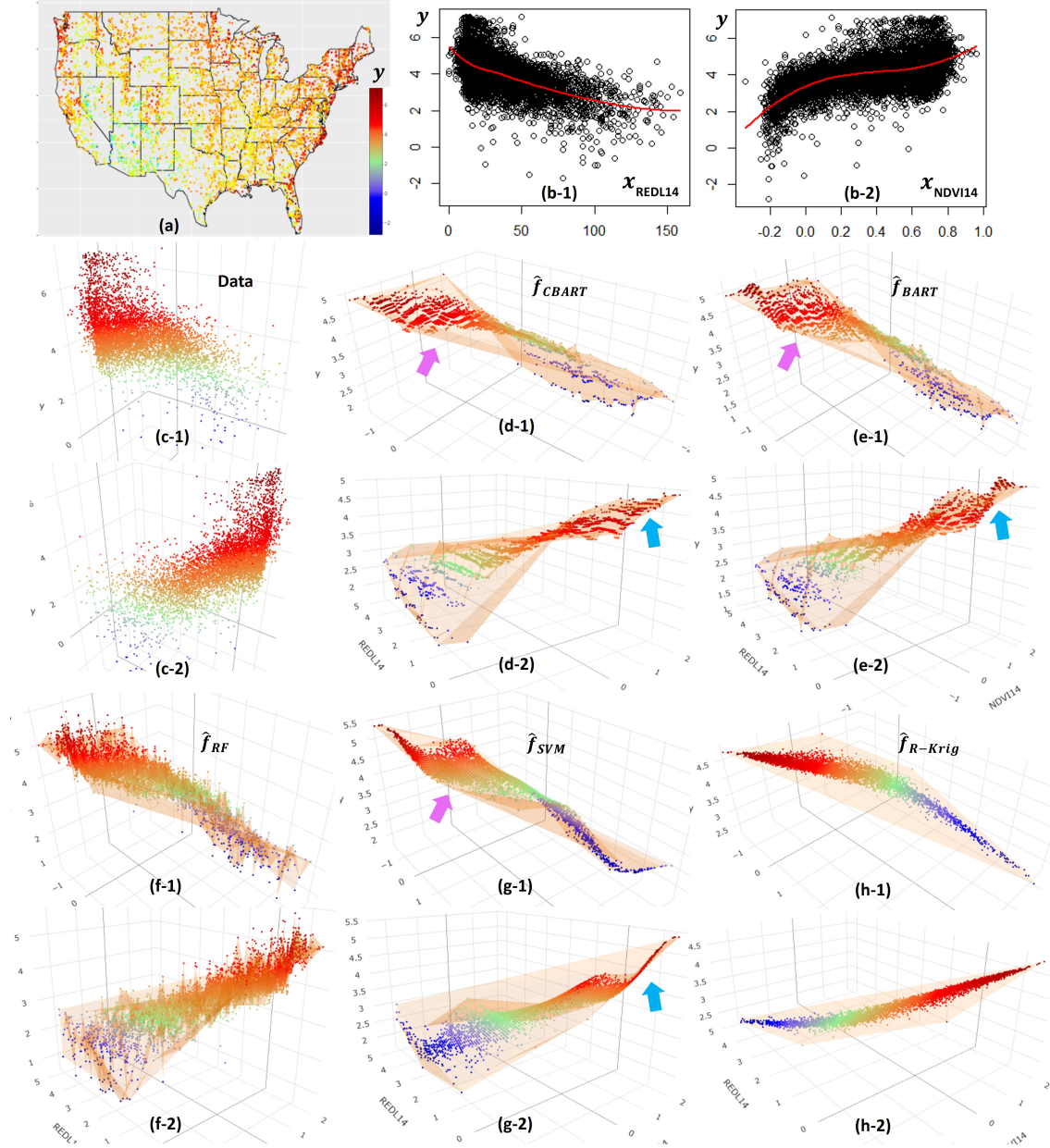


Figure 8: Real data analysis. (a) The spatial distribution of the response observations. (b-1,2) Two covariates have nonlinear relationship with response (different angles). (c-1,2) Observations in the 3 dimensional space defined by the response and covariates variables. (d-1,2) CBART's estimation of  $f(\mathbf{x})$ . (e-1,2) BART's estimation of  $f(\mathbf{x})$ . (f-1,2) RF's estimation of  $f(\mathbf{x})$ . (g-1,2) SVM's estimation of  $f(\mathbf{x})$ . (h-1,2) R-Krig's estimation of  $f(\mathbf{x})$ .

shown in panels (e-1,2), and (f-1,2). The  $\hat{f}_{BART}$  and  $\hat{f}_{RF}$  appear different from  $\hat{f}_{CBART}$  in panels (d-1,2), particularly in the regions indicated by the arrows. The differences

Table 2: The result of two-stage analysis of variance with weighted residuals.

$w_k$	0	0.2	0.4	0.6	0.8	<b>1</b>
$SS\Delta^k$	2408	2221	1874	1378	717	<b>95</b>

were caused by the spatial dependency of the observations. Thus, the following question is whether the spatial dependency is significant or not. This can be evaluated through the estimation of  $\theta = \{\sigma^2, \phi, \tau^2\}$ . We use the two-stage analysis of variance with weighted residuals to estimate  $\theta$ . As shown in Figure 3, we need to select the minimal  $SS\Delta^k$ . In Table 2, this corresponds to  $w_k = 1$ , indicating strong spatial dependency in the data. Therefore, we prefer the estimation of  $\hat{f}_{CBART}$  over  $\hat{f}_{BART}$  or  $\hat{f}_{SVM}$ . In other word,  $\hat{f}_{CBART}$ , as shown in panels (d-1,2), offers a more accurate interpretation of the relationship between the covariates  $x_{REDL14}$ ,  $x_{NDVI14}$  and response  $y$ .

## 6 Discussion

The original BART model has demonstrated effectiveness in identifying nonlinear relationships between a dependent variable and predictors, under the assumption of i.i.d. normal errors. This assumption is critical for maintaining MCMC efficiency, as it allows computations to focus on simple summary statistics in the few bottom nodes of each tree. In this paper, we develop a computational approach for running a BART-like MCMC while conditioning on normal errors with a general  $n \times n$  covariance matrix, where  $n$  is the number of observations. We represent a tree model with a linear dummy variable representation, where the dummies indicate the bottom nodes and the linear coefficients represent the bottom node mean parameters. Leveraging this representation and the error covariance, we structure the computations using linear algebra derived from a Bayesian analysis of the linear regression model. Then, crucially, given our dummy variable representation, we arrange the computations to make the MCMC feasible. We refer to this model and its computational approach as CBART (Correlated BART). Given CBART, we extend the model to incorporate dependent structures in the errors, introducing CBART-GP. In this approach,

the covariate-dependent mean is captured by CBART, while any remaining dependence in the errors is modeled using a Gaussian process.

Other approaches, such as tGP and GP-BART, have been developed to harness the strengths of BART and Gaussian processes by placing the Gaussian processes in the bottom nodes of trees. This configuration enhances the ability to detect local dependencies. However, these methods face a significant computational burden, given by  $O(N_{GP} \times N_{MCMC} \times N_{leaves})$ , where  $N_{GP}$  represents the computational complexity related to the GP that can be  $O(n^3)$  or  $O(n)$ ;  $N_{MCMC}$  is the number of MCMC iterations;  $N_{leaves} = m \times b_{avg}$  is the total number of bottom nodes (i.e., the number of trees  $m$  times the average number of leaves  $b_{avg}$  in each tree). This computational complexity may limit their applicability to large or even medium-sized datasets (e.g., 1000 samples). We propose a two-stage estimation approach for CBART-GP that is both simple and effective. This method involves running a small number of standard GP and CBART estimations (fewer than 10), significantly reducing the computational load from  $O(N_{MCMC} \times N_{leaves} \times N_{GP})$  to  $O(N_{GP})$ . This reduction is particularly noteworthy since  $N_{MCMC} \times N_{leaves}$  is typically quite large ( $\geq O(10^6)$ ). Beyond computational efficiency, CBART-GP is attractive because it bridges the gap between regression Kriging models, which are limited to estimating linear covariate regression functions, and popular nonparametric or machine learning models, which typically cannot account for the dependency structure in the data. CBART-GP has great potential for analyzing dependent data, such as time series and spatial data.

We found that running a full MCMC for CBART-GP was challenging due to the high computational complexity and the flexibility of both the CBART and GP components. Future work on this direction will focus on improving algorithm efficiency and exploring suitable priors to stabilize the full inference process.

## A Proofs

*Proof of Theorem 2.2.* Given (12), the product of likelihood and prior is as follows:

$$\begin{aligned}
p(R|D, \mu)\pi(\mu) &= (2\pi)^{-\frac{n}{2}} |\Sigma|^{-\frac{1}{2}} \exp\left\{-\frac{1}{2}(R - D\mu)^T \Sigma^{-1}(R - D\mu)\right\} * \\
&\quad (2\pi)^{-\frac{b}{2}} |Q|^{\frac{1}{2}} \exp\left\{-\frac{1}{2}(\mu - \bar{\mu})^T Q(\mu - \bar{\mu})\right\} \\
&= (2\pi)^{-\frac{n+b}{2}} |\Sigma|^{-\frac{1}{2}} |Q|^{\frac{1}{2}} * \\
&\quad \exp\left\{-\frac{1}{2} \underbrace{[(R - D\mu)^T \Sigma^{-1}(R - D\mu) + (\mu - \bar{\mu})^T Q(\mu - \bar{\mu})]}_{(*)}\right\}.
\end{aligned} \tag{28}$$

where,

$$\begin{aligned}
(*) &= R^T \Sigma^{-1} R - 2R^T \Sigma^{-1} D\mu + \mu^T D^T \Sigma^{-1} D\mu + \mu^T Q\mu - 2\bar{\mu}^T Q\mu + \bar{\mu}^T Q\bar{\mu} \\
&= \mu^T (D^T \Sigma^{-1} D + Q)\mu - 2(R^T \Sigma^{-1} D + \bar{\mu}^T Q)\mu + R^T \Sigma^{-1} R + \bar{\mu}^T Q\bar{\mu}.
\end{aligned}$$

Let's introduce a variable  $v$  and consider the quadratic form:

$$\begin{aligned}
&(\mu - v)^T (D^T \Sigma^{-1} D + Q)(\mu - v) \\
&= \mu^T (D^T \Sigma^{-1} D + Q)\mu - 2v^T (D^T \Sigma^{-1} D + Q)\mu + v^T (D^T \Sigma^{-1} D + Q)v.
\end{aligned}$$

With the equivalence constraint of above underline coefficients,  $v^T (D^T \Sigma^{-1} D + Q) = R^T \Sigma^{-1} D + \bar{\mu}^T Q$ , we can obtain that

$$v = (Q + D^T \Sigma^{-1} D)^{-1} (Q\bar{\mu} + D^T \Sigma^{-1} R). \tag{29}$$

Therefore,  $(*) = (\mu - v)^T (Q + D^T \Sigma^{-1} D)(\mu - v) + C$ , where

$$C = -v^T (Q + D^T \Sigma^{-1} D)v + R^T \Sigma^{-1} R + \bar{\mu}^T Q\bar{\mu}.$$

Then, plug  $(*)$  into (28):

$$\begin{aligned}
p(R|D) &= \int p(R|D, \mu)p(\mu)d\mu \\
&= (2\pi)^{-\frac{n+b}{2}} |\Sigma|^{-\frac{1}{2}} |Q|^{\frac{1}{2}} \exp\left\{-\frac{1}{2}C\right\} \int \exp\left\{-\frac{1}{2}(\mu - v)^T (Q + D^T \Sigma^{-1} D)(\mu - v)\right\} d\mu \\
&= (2\pi)^{-\frac{n+b}{2}} |\Sigma|^{-\frac{1}{2}} |Q|^{\frac{1}{2}} \exp\left\{-\frac{1}{2}C\right\} (2\pi)^{\frac{b}{2}} |Q + D^T \Sigma^{-1} D|^{-\frac{1}{2}} \\
&\quad \cdot \int (2\pi)^{-\frac{b}{2}} |Q + D^T \Sigma^{-1} D|^{\frac{1}{2}} \exp\left\{-\frac{1}{2}(\mu - v)^T (Q + D^T \Sigma^{-1} D)(\mu - v)\right\} d\mu \\
&= \frac{(2\pi)^{-\frac{n}{2}} |\Sigma|^{-\frac{1}{2}} |Q|^{\frac{1}{2}}}{|Q + D^T \Sigma^{-1} D|^{\frac{1}{2}}} \exp\left\{-\frac{1}{2}C\right\}
\end{aligned}$$



After simplification, we can get the expression in (13).

$$p(R|D) = \frac{(2\pi)^{-\frac{n}{2}} |\Sigma|^{-\frac{1}{2}} |Q|^{\frac{1}{2}}}{|Q + D^T \Sigma^{-1} D|^{\frac{1}{2}}} \exp\left\{-\frac{1}{2}(-v^T(Q + D^T \Sigma^{-1} D)v + \bar{\mu}^T Q \bar{\mu} + R^T \Sigma^{-1} R)\right\},$$

where  $v = (Q + D^T \Sigma^{-1} D)^{-1}(Q \bar{\mu} + D^T \Sigma^{-1} R)$ .  $\square$

*Proof of Theorem 2.3.* Given  $D$  and  $\Sigma$ , the posterior distribution of  $\mu$  is proportional to the product of its likelihood and prior as follows:

$$p(\mu|R) \propto p(R|\mu)\pi(\mu) = p(R|D, \mu)\pi(\mu), \quad (30)$$

where  $p(R|D, \mu) \sim N(D\mu, \Sigma)$  and  $\pi(\mu) \sim N(\bar{\mu}, Q^{-1})$ .

Then, conduct the same derivation in (28) and (29), we can prove that

$$p(\mu|R) \sim N((Q + D^T \Sigma^{-1} D)^{-1}(Q \bar{\mu} + D^T \Sigma^{-1} R), (Q + D^T \Sigma^{-1} D)^{-1}). \quad (31)$$

$\square$

*Proof of Theorem 2.5.* Since  $P$  is a permutation matrix, it has the property  $P^{-1} = P^T$ .

With (19) and (20), we can obtain the following:

$$\begin{aligned} D^T \Sigma^{-1} R &= (PD_P)^T (P \Sigma_P P^T)^{-1} (PR_P) \\ &= D_P^T P^T P \Sigma_P^{-1} P^T P R_P \\ &= D_P^T \Sigma_P^{-1} R_P \end{aligned} \quad (32)$$

Given  $Q = \tau^{-2}I$ , we can get

$$Q + D^T \Sigma^{-1} D = Q + (PD_P)^T P \Sigma_P^{-1} P^T P D_P = Q + D_P^T \Sigma_P^{-1} D_P. \quad (33)$$

Plug (20), (32), (33) into (15), we can prove the theorem is hold.

$$\begin{aligned} \frac{p(R|D^{i+1})}{p(R|D^i)} &= \frac{|Q^{i+1}|^{\frac{1}{2}}}{|Q^i|^{\frac{1}{2}}} \frac{|Q^i + (D^i)^T \Sigma^{-1} D^i|^{\frac{1}{2}}}{|Q^{i+1} + (D^{i+1})^T \Sigma^{-1} D^{i+1}|^{\frac{1}{2}}} \cdot \exp\left\{\frac{1}{2} R^T \Sigma^{-1} [D^{i+1}(Q^{i+1} + \right. \\ &\quad \left. (D^{i+1})^T \Sigma^{-1} D^{i+1})^{-1} (D^{i+1})^T - D^i(Q^i + (D^i)^T \Sigma^{-1} D^i)^{-1} (D^i)^T] \Sigma^{-1} R\right\} \\ &= \frac{|Q^{i+1}|^{1/2}}{|Q^i|^{1/2}} \frac{|Q^i + (D_P^i)^T \Sigma_P^{-1} D_P^i|^{1/2}}{|Q^{i+1} + (D_P^{i+1})^T \Sigma_P^{-1} D_P^{i+1}|^{1/2}} \cdot \exp\left\{\frac{1}{2} R_P^T \Sigma_P^{-1} [D_P^{i+1}(Q^{i+1} + \right. \\ &\quad \left. (D_P^{i+1})^T \Sigma_P^{-1} D_P^{i+1})^{-1} (D_P^{i+1})^T - D_P^i(Q^i + (D_P^i)^T \Sigma_P^{-1} D_P^i)^{-1} (D_P^i)^T] \Sigma_P^{-1} R_P\right\} \end{aligned}$$

$\square$

## B Marginal likelihood ratio calculation

Updating  $T$  in (7) involves two node operations: birth and death. Birth entails the creation of two child nodes from a leaf node, while death involves removing the two sibling leaf nodes from their parent. For both operations, we need to calculate the marginal likelihood ratio, which includes the following three steps.

### (1) Calculate matrix $A$

By (18) and (33), we know

$$A = Q + D_P^T \Sigma_P^{-1} D_P,$$

where  $Q = \tau^{-2}I$ .

$A$  is a symmetric matrix and can be denoted as follows:

$$A = \begin{bmatrix} a_{11} + \tau^{-2} & a_{12} & \dots & a_{1b} \\ a_{21} & a_{22} + \tau^{-2} & \dots & a_{2b} \\ \vdots & \vdots & \ddots & \vdots \\ a_{b1} & a_{b2} & \dots & a_{bb} + \tau^{-2} \end{bmatrix}, \quad (34)$$

where

$$a_{ji} = a_{ij} = \sum_{h \in \Omega_i} \sum_{l \in \Omega_j} q_{hl}, \quad i \leq j, \quad i, j \in \{1, \dots, b\}.$$

$\Omega_i$  and  $\Omega_j$  are the index sets of observations that are associated with bottom nodes  $i$  and

$j$ ;  $q_{hl}$  is the entry at the intersection of  $h^{th}$  row and  $l^{th}$  column in matrix  $\Sigma_P^{-1}$  as follows:

$$\Sigma_P^{-1} = \begin{bmatrix} q_{11} & q_{12} & \cdots & q_{1n} \\ q_{21} & q_{22} & \cdots & q_{2n} \\ \vdots & \vdots & \ddots & \vdots \\ q_{n1} & q_{n2} & \cdots & q_{nn} \end{bmatrix}$$

## (2) Calculate the block matrix $\mathbf{E}$

Plugging  $A$  into (21), we can get

$$\begin{aligned} \frac{p(R|D^{i+1})}{p(R|D^i)} &= \frac{|Q^{i+1}|^{1/2}}{|Q^i|^{1/2}} \frac{|A^i|^{1/2}}{|A^{i+1}|^{1/2}} \\ &\cdot \exp\left\{\frac{1}{2} R_P^T \Sigma_P^{-1} \underbrace{[D_P^{i+1}(A^{i+1})^{-1}(D_P^{i+1})^T - D_P^i(A^i)^{-1}(D_P^i)^T]}_E \Sigma_P^{-1} R_P\right\}. \end{aligned}$$

To calculate  $E$ , we need to consider the birth and death operations separately. Without loss of generality, let's assume that the birth or death operation occurs in the  $(i+1)^{th}$  MCMC iteration.

### Birth

In birth operation, the tree has  $b$  bottom nodes at  $i^{th}$  iteration and  $b+1$  bottom nodes at  $(i+1)^{th}$  iteration. The corresponding  $(A^i)^{-1}$  and  $(A^{i+1})^{-1}$  are  $b \times b$  and  $(b+1) \times (b+1)$  matrices. We can denote them by block matrices as follows:

$$(A^{i+1})^{-1} = \begin{bmatrix} V_{11}^{i+1} & V_{12}^{i+1} \\ V_{21}^{i+1} & V_{22}^{i+1} \end{bmatrix}, \quad (A^i)^{-1} = \begin{bmatrix} V_{11}^i & v_{12}^i \\ v_{21}^i & v_{22}^i \end{bmatrix}$$

where,  $V_{11}^{i+1}$  and  $V_{11}^i$  are  $(b-1) \times (b-1)$  matrices;  $V_{12}^{i+1} = (V_{21}^{i+1})^T$  is  $(b-1) \times 2$  matrix;  $v_{12}^i = v_{21}^i$  is a  $b-1$  column vector;  $v_{22}^i$  is a scalar.

We create a matrix

$$(A^i)_{ex}^{-1} = \begin{bmatrix} V_{11}^i & v_{12}^i & v_{12}^i \\ v_{21}^i & v_{22}^i & v_{22}^i \\ v_{21}^i & v_{22}^i & v_{22}^i \end{bmatrix}$$

Let  $B = (A^{i+1})^{-1} - (A^i)_{ex}^{-1}$ , then we can get

$$B = \begin{bmatrix} V_{11}^{i+1} - V_{11}^i & V_{12}^{i+1} - \begin{bmatrix} v_{12}^i & v_{12}^i \end{bmatrix} \\ V_{21}^{i+1} - \begin{bmatrix} v_{21}^i \\ v_{21}^i \end{bmatrix} & V_{22}^{i+1} - \begin{bmatrix} v_{22}^i & v_{22}^i \\ v_{22}^i & v_{22}^i \end{bmatrix} \end{bmatrix} = \begin{bmatrix} b_{11} & b_{12} & \dots & b_{1(b+1)} \\ b_{21} & b_{22} & \dots & b_{2(b+1)} \\ \vdots & \vdots & \ddots & \vdots \\ b_{(b+1)1} & b_{(b+1)2} & \dots & b_{(b+1)(b+1)} \end{bmatrix}$$

## Death

Similar to the birth operation, we have  $(A^i)^{-1}$  and  $(A^{i+1})^{-1}$  as follows:

$$(A^i)^{-1} = \begin{bmatrix} V_{11}^i & V_{12}^i \\ V_{21}^i & V_{22}^i \end{bmatrix}, \quad (A^{i+1})^{-1} = \begin{bmatrix} V_{11}^{i+1} & v_{12}^{i+1} \\ v_{21}^{i+1} & v_{22}^{i+1} \end{bmatrix}$$

where  $V_{11}^{i+1}$  and  $V_{11}^i$  are  $(b-2) \times (b-2)$  matrices;  $V_{12}^i = (V_{21}^i)^T$  is  $(b-2) \times 2$  matrix;  $v_{12}^{i+1} = v_{21}^{i+1}$  is a  $b-2$  column vector;  $v_{22}^{i+1}$  is a scalar.

Create a matrix

$$(A^{i+1})_{ex}^{-1} = \begin{bmatrix} V_{11}^{i+1} & v_{12}^{i+1} & v_{12}^{i+1} \\ v_{21}^{i+1} & v_{22}^{i+1} & v_{22}^{i+1} \\ v_{21}^{i+1} & v_{22}^{i+1} & v_{22}^{i+1} \end{bmatrix}$$

In this case,  $B = (A^{i+1})_{ex}^{-1} - (A^i)^{-1}$  as follows:

$$B = \begin{bmatrix} V_{11}^{i+1} - V_{11}^i & \begin{bmatrix} v_{12}^{i+1} & v_{12}^{i+1} \end{bmatrix} - V_{12}^i \\ \begin{bmatrix} v_{21}^{i+1} \\ v_{21}^{i+1} \end{bmatrix} - V_{21}^i & \begin{bmatrix} v_{22}^{i+1} & v_{22}^{i+1} \\ v_{22}^{i+1} & v_{22}^{i+1} \end{bmatrix} - V_{22}^i \end{bmatrix} = \begin{bmatrix} b_{11} & b_{12} & \dots & b_{1b} \\ b_{21} & b_{22} & \dots & b_{2b} \\ \vdots & \vdots & \ddots & \vdots \\ b_{b1} & b_{b2} & \dots & b_{bb} \end{bmatrix}$$

**Block matrix E**

$$E = D_P^{i+1}(A^{i+1})^{-1}(D_P^{i+1})^T - D_P^i(A^i)^{-1}(D_P^i)^T = \begin{bmatrix} E_{11} & E_{12} & \dots & E_{1b'} \\ E_{21} & E_{22} & \dots & E_{2b'} \\ \vdots & \vdots & \ddots & \vdots \\ E_{b'1} & E_{b'2} & \dots & E_{b'b'} \end{bmatrix}$$

where the  $b'$  in the subscript of the block matrices  $E_{ij}$  is

$$b' = \begin{cases} b + 1, & \text{Birth,} \\ b, & \text{Death.} \end{cases}$$

and, each block  $E_{ij}$  has a special form as follows:

$$E_{ij} = E_{ji}^T = b_{ij}\mathbb{J}_{ij}, \quad i \leq j, \quad i, j \in \{1, \dots, b'\}$$

where  $b_{ij}$  is the  $(i, j)$  entry of matrix  $B$  calculated in the birth or death step;  $\mathbb{J}_{ij}$  is a  $\text{card}(\Omega_i) \times \text{card}(\Omega_j)$  matrix whose entries are all 1. The special form of  $\mathbb{J}_{ij}$  reduces the computation load of calculating matrix  $E$  from  $O(n^2)$  to  $O(b^2)$ .

### (3) Calculate marginal likelihood ratio

Let's set

$$R_P^T \Sigma_P^{-1} = \begin{bmatrix} \omega_1 & \omega_2 & \dots & \omega_{b'} \end{bmatrix}, \quad \omega_i = [\omega_{ij}], \quad j \in n_i$$

and

$$u = R_P^T \Sigma_P^{-1} E \Sigma_P^{-1} R_P.$$

Then,  $u$  can be calculated as follows:

$$\begin{aligned} u &= \begin{bmatrix} \omega_1 & \omega_2 & \dots & \omega_{b'} \end{bmatrix} E \begin{bmatrix} \omega_1^T \\ \omega_2^T \\ \vdots \\ \omega_{b'}^T \end{bmatrix} \\ &= \sum_{i=1}^{b'} \sum_{j=1}^{b'} \omega_i E_{ij} \omega_j^T \\ &= \sum_{i=1}^{b'} \sum_{j=1}^{b'} (\omega_i \mathbb{J}_{ij} \omega_j^T) b_{ij} \\ &= \sum_{i=1}^{b'} \sum_{j=1}^{b'} [(\sum_{h \in n_i} \omega_{ih})(\sum_{l \in n_j} \omega_{jl}) b_{ij}]. \end{aligned}$$

Finally, we can get the marginal likelihood ratio as follows:

$$\frac{p(R|D^{i+1})}{p(R|D^i)} = \begin{cases} \tau^{-1} \frac{|A^i|}{|A^{i+1}|} \exp\{\frac{1}{2}u\} & \text{Birth} \\ \tau \frac{|A^i|}{|A^{i+1}|} \exp\{\frac{1}{2}u\} & \text{Death.} \end{cases}$$

The computation load in step (3) is  $O(n)$ . Thus, the computation complexity of marginal likelihood ratio (21) calculation is  $\max\{O(n), O(b^2)\}$ .

## References

- Brahim-Belhouari, S. and A. Bermak (2004). Gaussian process for nonstationary time series prediction. *Computational Statistics & Data Analysis* 47(4), 705–712.
- Chipman, H., E. George, and R. McCulloch (2006). Bayesian ensemble learning. In B. Schölkopf, J. Platt, and T. Hoffman (Eds.), *Advances in Neural Information Processing Systems*, Volume 19. MIT Press.
- Chipman, H. A., E. I. George, and R. E. McCulloch (1998). Bayesian cart model search. *Journal of the American Statistical Association* 93(443), 935–948.
- Chipman, H. A., E. I. George, and R. E. McCulloch (2010). Bart: Bayesian additive regression trees. *The Annals of Applied Statistics* 4, 266–298.
- Cressie, N. (1993). *Statistics for Spatial Data*, pp. 1–26. John Wiley & Sons, Ltd.
- Datta, A., S. Banerjee, A. O. Finley, and A. E. Gelfand (2016). Hierarchical nearest-neighbor gaussian process models for large geostatistical datasets. *Journal of the American Statistical Association* 111(514), 800–812.
- Finley, A. O., A. Datta, B. D. Cook, D. C. Morton, H. E. Andersen, and S. Banerjee (2019). Efficient algorithms for bayesian nearest neighbor gaussian processes. *Journal of Computational and Graphical Statistics* 28(2), 401–414.
- George, E., P. Laud, B. Logan, R. McCulloch, and R. Sparapani (2019). Fully Nonparametric Bayesian Additive Regression Trees. In I. Jeliaskov and J. L. Tobias (Eds.), *Topics in Identification, Limited Dependent Variables, Partial Observability, Experimentation, and Flexible Modeling: Part B*, Volume 40 of *Advances in Econometrics*, pp. 89–110. Emerald Publishing Ltd.
- Gramacy, R. B. and H. K. Lee (2008). Bayesian treed gaussian process models with an application to computer modeling. *Journal of the American Statistical Association* (103), 1119–1130.
- Hackbusch, W. (2015). *Hierarchical Matrices: Algorithms and Analysis* (1st ed.). Springer Publishing Company, Incorporated.



- Hastie, T. and R. Tibshirani (2000). Bayesian backfitting. *Statistical Science* 15(3), 196–213.
- Hill, J. L., A. R. Linero, and J. Murray (2020). Bayesian additive regression trees: A review and look forward. *Annual Review of Statistics and Its Application*.
- Krige, d. g. (1951). *A Statistical Approach to Some Mine Valuation and Allied Problems on the Witwatersrand*.
- Lin, L., J. Lu, and L. Ying (2011). Fast construction of hierarchical matrix representation from matrix–vector multiplication. *Journal of Computational Physics* 230(10), 4071–4087.
- Litvinenko, A., Y. Sun, M. G. Genton, and D. E. Keyes (2019). Likelihood approximation with hierarchical matrices for large spatial datasets. *Computational Statistics and Data Analysis* 137, 115–132.
- Maia, M., K. Murphy, and A. C. Parnell (2024). Gp-bart: A novel bayesian additive regression trees approach using gaussian processes. *Computational Statistics and Data Analysis*.
- Piegorsch, W. W., R. A. Levine, H. H. Zhang, and T. C. M. Lee (2022). *Computational Statistics in Data Science*. Wiley.
- Pratola, M. T., H. A. Chipman, E. I. George, and R. E. McCulloch (2020). Heteroscedastic bart via multiplicative regression trees. *Journal of Computational and Graphical Statistics* 29(2), 405–417.
- Rasmussen, C. E. and C. K. I. Williams (2005, 11). *Gaussian Processes for Machine Learning*. The MIT Press.
- Roberts, S. J., M. A. Osborne, M. Ebden, S. Reece, N. P. Gibson, and S. Aigrain (2012). Gaussian processes for timeseries modelling.
- Starling, J. E., J. S. Murray, C. M. Carvalho, R. K. Bukowski, and J. G. Scott (2020). Bart with targeted smoothing: An analysis of patient-specific stillbirth risk. *Annals of Applied Statistics* 14(1), 28 – 50. Cited by: 16; All Open Access, Bronze Open Access, Green Open Access.

Stein, A. and L. C. A. Corsten (1991). Universal kriging and cokriging as a regression procedure. *Biometrics* 47(2), 575–587.

Wijewardane, N. K., Y. Ge, S. Wills, and T. Loecke (2016). Prediction of soil carbon in the conterminous united states: Visible and near infrared reflectance spectroscopy analysis of the rapid carbon assessment project. *Soil Science Society of America Journal* 80(4), 973–982.